Trócoli, Rafael ; Morata, Alex ; Erinmwingbovo, Collins ; La Mantia, Fabio ; Tarancón, Albert

⊞

Self-discharge in Li-ion aqueous batteries: A case study on LiMn2O4

Recommended Citation (primary publication/Version of Record) incl. DOI:

R. Trócoli, A. Morata, C Erinmwingbovo, F. La Mantia, A. Tarancón,
Self-discharge in Li-ion aqueous batteries: A case study on LiMn2O4,
Electrochimica Acta, Volume 373, 2021, 137847, ISSN 0013-4686,
https://doi.org/10.1016/j.electacta.2021.137847.

⊞

Take down policy
If you believe that this document or any material on this site infringes copyright, please contact
publizieren@suub.uni-bremen.de with full details and we will remove access to the material.

Self-discharge in Li-ion aqueous batteries: A case study on LiMn$_2$O$_4$

R. Trócoli [a,b,*], A. Morata [b], C Erinmwingbovo [c], F. La Mantia [c], A. Tarancón [b,*]

[a] *Instituto de Ciencias de Materiales de Barcelona (ICMAB-CSIC), Campus UAB, E-08193, Bellaterra, Catalonia, Spain*
[b] *IREC, Jardins de les Dones de Negre 1, 2a 08930 Sant Adriá de Besós, Barcelona, Spain*
[c] *Universität Bremen, Energiespeicher-und Energiwandlersyteme, Bibliothekstr. 1, 28359 Bremen, Germany*

ARTICLE INFO

ABSTRACT

Aqueous rechargeable lithium-ion batteries have attracted great attention as an alternative to traditional battery technologies, being able to overcome the issues caused by flammable and expensive organic electrolytes. In particular, LiMn$_2$O$_4$ has reached very fast second-level charge capability by the synthesis of unconventional morphology and particle sizes, allowing charging rates up to 600 C and 93% retention of the capacity after 10,000 cycles. However, the self-discharge process and aging mechanisms for aqueous batteries have been rarely studied, which contrasts with the extensive bibliography of the same phenomena in LMO cells based on organic electrolytes. In this article, the mechanisms involved in the loss of reversible specific charges were studied by diverse techniques like OCV, EIS, and In-situ Raman. The results revealed a more favorable self-discharge process compared with using organic electrolytes owing to the lower stability of water. The self-discharge process can be divided into three different regions with a sequential lower decay rate of voltage and capacity as well as two different evolutions of the electric parameters. This study opens new questions about the nature, composition, and mechanisms of the self-discharge in aqueous media which will play a critical role in the electrochemical performance of novel aqueous Li-ion batteries.

1. Introduction

The development of highly variable renewable energy sources like wind or solar powers will require a considerable increment in the large-scale energy storage capabilities to enable their integration into the power grid. Currently, battery technologies do not fill the needed requirements in terms of costs, power, and/or durability [1–5]. Recently aqueous rechargeable lithium-ion batteries (ARLB) have attracted great attention as an alternative to traditional technologies, able to overcome the issues caused by the use of organic electrolytes (flammable and expensive) owing to their environmentally friendly chemistry, low-cost, and safety [6]. The use of classic (de-)intercalation electrodes is restricted to materials with redox potential between the oxidation and reduction limits of water. Among different studied cathodes, LiMn$_2$O$_4$ (LMO) has stood out as an ideal candidate offering high discharge voltage with low cost and toxicity. Contrary to the initial studies, in the early 2000th, where ARLB batteries provided limited capacity and stability [7–11], in recent studies, the named "Second-Level Charge Capability" has been reached by the synthesis of LMO with unconventional particle sizes and morphologies. Tang´s group reported nanorods [12], nanotubes [13] nanochains [14,15], and nanocomposites MoO$_3$-PPY@LMO [16] charged up to 600 C, while Wu et al. prepared porous LMO with retention of the capacity of 93% after 10,000 cycles. [17] Also, owing to its fast lithium (de-)intercalation in aqueous electrolyte LMO has been even employed as a supercapacitor [18–21]. Recently, our group has prepared several LMO thin film samples with similar electrochemical responses than these super-fast material being cycled up to 348 C for more than 3500 cycles [22–26].

On the other hand, the decrease in the available capacity with storage time associated with the self-discharge is inherent in batteries [27]. The specific charge loss depends mostly on the cell components' nature, the state of charge (SOC), and storing conditions. However, other characteristics of the battery like material purity or high specific surface area of the components (active and inactive) could play a critical role. The self-discharge occurs when one and/or both electrodes are not within the thermodynamic stability window of the electrolyte, which is then oxidized or reduced at the cathode or anode sides respectively. These reactions imply a loss of specific charge that could be or not recovered for the posterior battery cycling and cause a decrease in the open-circuit voltage (OCV). Unlike LMO cells based on organic electrolytes, where the reversible and irreversible self-discharge processes and aging
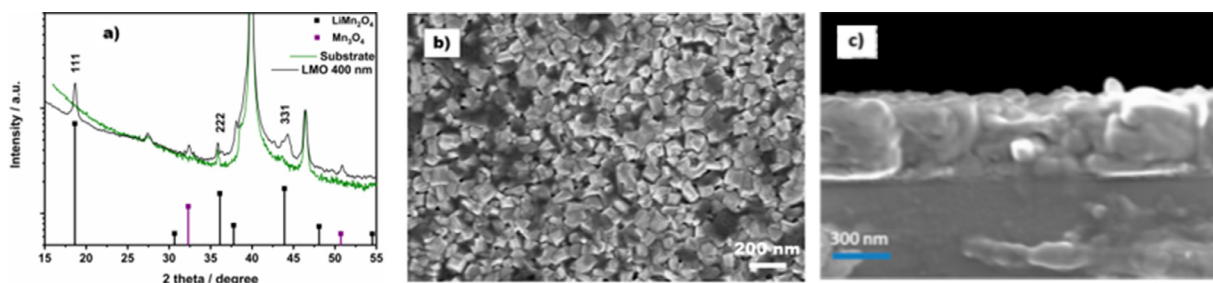

Fig. 1. XRD diffractogram of LMO thin film (a). Top (b) and cross-section (c) SEM images of the film.
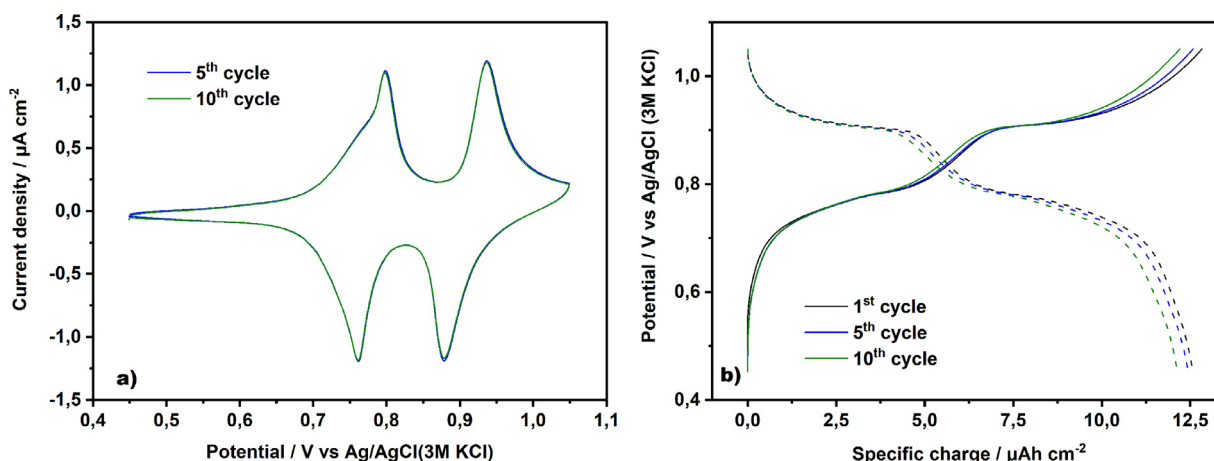

Fig. 2. Cyclic voltammetry (a) and constant current (b) measurements of LMO thin films. A three electrodes cell configuration was employed using Pt mesh and Ag/AgCl (3 M KCl) as counter and reference electrodes respectively.

mechanisms have been extensively studied [28–36], scarce bibliography can be found for LMO aqueous batteries. To the best of our knowledge, just Konarov et al. reported the effect of the specific surface area of the conducting agent and the acid condition of the electrolyte in the Mn dissolution [37]. Therefore, a deeper understanding of the self-discharge process is required. In this article, we have evaluated the self-discharge of LMO thin films prepared by Pulsed Laser Deposition. The mechanisms involved in the loss of reversible specific charge were studied by diverse techniques as Electrochemical Impedance Spectroscopy and In-situ Raman analysis.

2. Experimental section

LMO thin films were prepared using a multilayer PLD method previously described in [23,24,26]. Briefly, LMO thin films were deposited using a Large Area PLD5000 by PVD Products, Inc. equipped with a KrF excimer laser with 248 nm wavelength by combinatorial deposition using LMO and Li_2O targets purchased from Neyco, France. Films were deposited onto Si/TiN(10 nm)/Pt (80 nm) substrates provided by Imec. The substrates were cleaned prior to deposition subsequently with acetone, mili-Q water, and isopropanol. The laser fluency was fixed at 650 mJ cm^{-2} and an oxygen background pressure of 20 mTorr was applied. The deposition temperature, target-substrate distance, and frequency were 650 °C, 90 mm, and 10 Hz, respectively. LMO and Li_2O materials were deposited alternatively in a pulse ratio of 2:1 until the desired 400 nm thicknesses were reached. A Bruker-D8 Advance equipment was used for XRD measurements applying an offset to avoid the substrate contribution (Si). The SEM images were obtained with a Zeiss Auriga. The electrochemical measurements were carried out using a tree electrodes configuration cell, specifically designed for thin film electrodes. [38,39]. Ag/AgCl 3 M KCl

and Pt mesh were used as the reference and the counter electrode respectively. All measurements were done under ambient air and temperature. 5 mV s^{-1} was employed as scan rate for the cyclic voltammetry (CV) measurements. A current density of 33.3 μA cm^{-2} was applied for the galvanostatic cycling. The potential window used for both, CV and GCPL, was from 0.45 to 1.05 V vs Ag/AgCl (3 M KCl). An Ag/AgCl (3M KCl) reference electrode capacitively coupled with a 100 nF capacitor was used for the impedance measurements (EIS). For the EIS, 10 mV peak to peak was used as an excitation signal over the range of 100 kHz–1 Hz. The EIS diagrams obtained were fitted with the software Zplot, from Scribner Associates. A HR800 (Horiba Jobin Yvon) was used for Raman measurement (532 nm excitation line) recording the wide spectral range (200–1400 cm^{-1}) every 5 minutes acquiring 160 scans. Labspec 6 and Origin software was used to analyze the Raman data.

3. Results and discussion

The prepared LMO thin films were prepared by Pulsed Laser Deposition (PLD) following the multilayer synthesis condition indicated in [23,24,26]. The LMO thin films (thickness of c.a. d=400 nm) were deposited on Si/TiN/Pt substrates. The deficient layers commonly obtained in the Li-based compounds prepared by PLD is due to the higher scattering of light species. To compensate for this deficiency, we have previously optimized a multilayer combinatorial approach based on the intercalated depositions of LMO and Li_2O layers which allow obtaining stoichiometric films [23,24,26]. Fig. 1a shows the X-ray diffraction spectra of the as-deposited LMO film, bare Si/TiN/Pt substrate was also included for comparison. The predominant phase in the film was clearly LMO cubic spinel phase (JCPDS 35-0782). A classic displacement caused by the stress typically founded in thin films deposited onto rigid substrates was observed in peaks at 36.132 (311) and 37.798 (222).
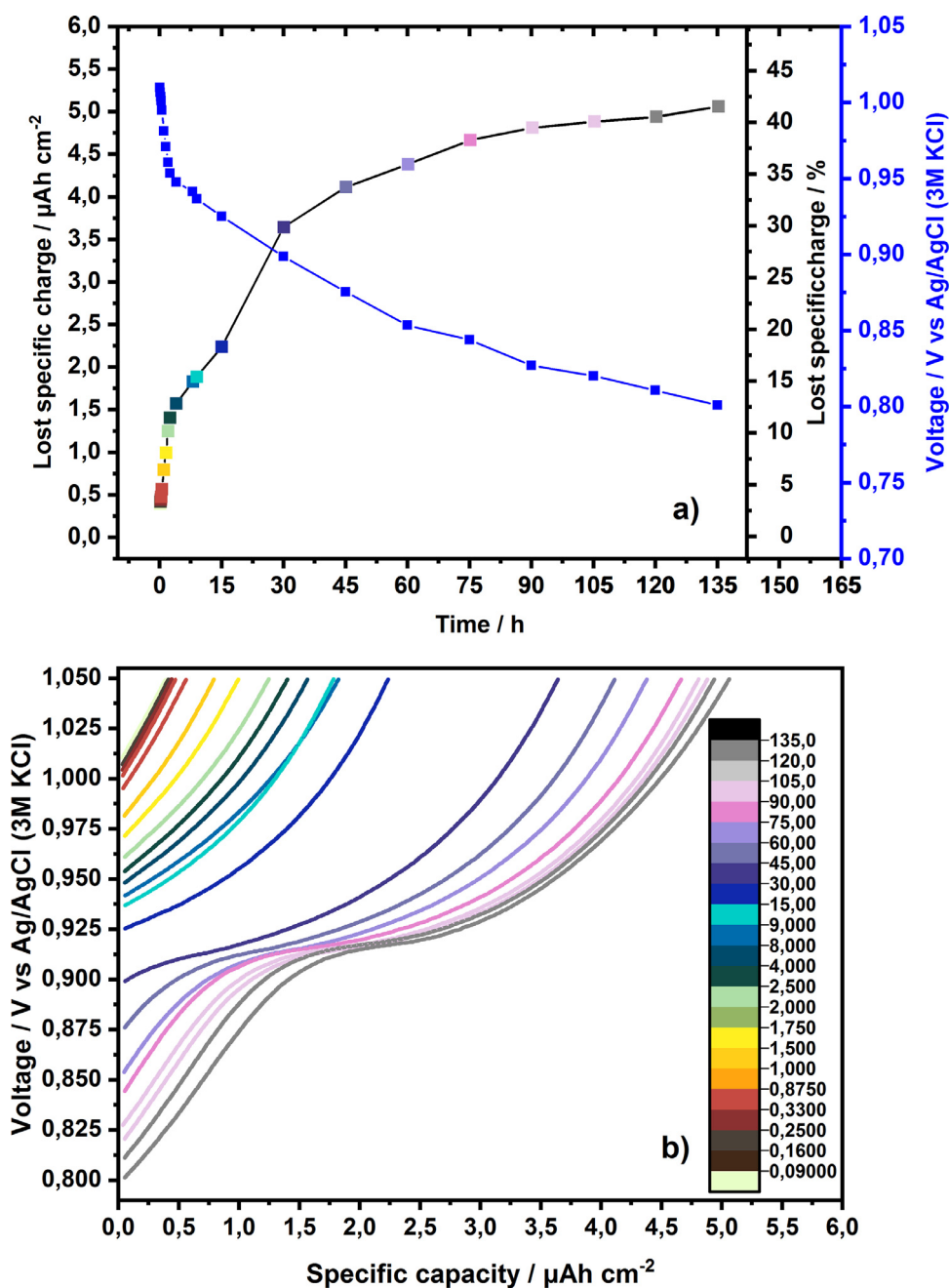
2

Fig. 3. Evolution of specific charge losses and potential with resting time a) and oxidation potential profile of LMO thin films after resting times.

Particles with rhombohedral shape and dimensions in the range from 50 nm to 80 nm were obtained, which coated completely the substrate (Fig. 1b and 1c), avoiding a possible exposition of the Pt current collector to the electrolyte which could cause undesired side-reactions (mainly water evolution catalyzed by the Pt).

Fig. 2 shows the classic electrochemical behavior reported for aqueous LMO batteries using fast kinetic LMO electrodes [22–24,26]. The two cyclic voltammetry peaks and equivalent plateaus in constant current measurements were associated with the (de-)intercalation of Li$^+$ from/into the spinel structure:

$$LiMn_2O_4 \leftrightarrow Li^+ + 2\ \lambda\text{-}MnO_2 \qquad (1)$$

The specific charge provided by the 400 nm-thick LMO films was equivalent to previous values reported in the literature [22–

24,26]. Before the self-discharge study, the thin films were cycled until the coulumbic efficient reached values superior to 99.5%. In general, a set of 10 CVs and 10 galvanostatic cycles were required.

To evaluate the losses of reversible specific capacity by self-discharge effect a three-steps protocol was followed: first the potential evolution of an oxidized LMO thin film was monitored by an open circuit potential measurement, the λ-MnO$_2$ was spontaneously converted into Li$_x$Mn$_2$O$_4$ (the time of this OCVs was sequentially increased); secondly an impedance spectroscopy measurement was applied, and finally the LMO thin films were charged to a cut off potential of 1.05 V vs. Ag/AgCl (3 M KCl). The specific charge provided during the oxidation step was considered equivalent to the specific charge lost owing to the previous self-discharge (OCV) of the film. The OCVs profiles obtained at different resting times are shown in Fig. 2 Sup. Inf. The first de-intercalation
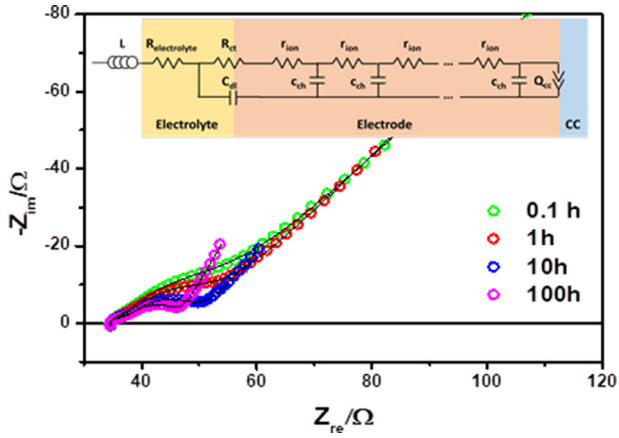
Fig. 4. Nyquist plot of the impedance measurements of the LMO layer during the self-discharge at t=0.1, 1, 10, and 100 h (open symbols). The insert shows the equivalent circuit employed for the fitting of the arcs (solid lines).

plateau was unmistakably observed at time superior to 15 h, on the contrary, the second plateau was not obtained even at times as high as 135 h. The evolution of the potential with the resting time can be divided into three regions (Fig. 3a). Initially, at times lower than 2.5 h, the potential drop quickly (22.5 mVh^{-1}) and the losses of specific charge associated with this potential drop reached a value of 11.5% of the total specific charge (4.6%h^{-1}). A smaller potential decrease was observed in the range from 2.5 to 60 h (1.7 mVh^{-1}), with an additional loss of specific charge of 24.4% (0.42% per hour). Finally, the third region was characterized by a very slow potential decay (0.7 mVh^{-1}), equivalent to a 5.6% lost specific charge (0.075%h^{-1}). These values of capacity losses were in agreement with the oxidation potential profiles obtained (Fig. 3b), just the highest potential plateau and the transition step between plateaus were observed which correspond to less than 45% of the total specific charge, therefore less than half of the Mn was reduced/oxidized.

It has been demonstrated that the LMO reversible self-discharge in classic Li-ion batteries using organic electrolyte was highly affected by two parameters: the presence of an anode electrode like Li or Carbon, when Pt was used as counter electrode the self-discharge process was unobserved; and the temperature of storage, at 55 °C the process was exacerbated. In all these cases the two plateaus associated with the intercalation of lithium were observed [28–36]. However, as Fig. 3b and Fig. 2. S. Inf. show, when

aqueous electrolytes were used just the first plateau was obtained (the counter electrode here was Pt).

Fig. 3 demonstrates that unlike using organic electrolytes, in Li-ion aqueous batteries a reversible self-discharge process occurs even at room temperature and using Pt as the anode electrode. The lower stability of water as electrolyte, the reduced activation energy for the interfacial Li-ion transfer reaction in aqueous solution [30], and the capacity of LMO species to catalyze water oxidation [40–42] could favor the self-discharge in Li-ion aqueous batteries. With the aim to monitor the evolution of critical parameters in LMO aqueous cells during the self-discharge process, impedance spectra were measured at each resting time. Fig. 4 shows representative Nyquist plots obtained during the self-discharge experiment at t=0.1, 1, 10, and 100 h. Higher resting times indicate higher self-discharges and displacements from left to the right of reaction 1. The change in the shape of the arcs can be directly correlated with the progressive insertion of the lithium in the electrode. By using a physically meaningful equivalent circuit [43–51] it is possible to quantitatively analyze the evolution of the most relevant parameters describing the system, namely, i) the charge transfer resistance (R_{ct}) and double layer capacitance (C_{dl}), which characterize the electrolyte-electrode interface; ii) the chemical capacitance (C_{chem}) and the ionic pathway resistance (R_{ion}) related to the change of Li stoichiometry and Li-ion diffusivity within the electrode, respectively; and iii) the back contact capacitance (Q_{cc}) corresponding to the accumulation of Li close to the LMO-current collector interface. The very same equivalent circuit was employed all along the whole discharge process to give coherence to the analysis and, despite this, the quality of the fitting (solid line in Fig. 4) was above the standards ($\chi^2 < 10^{-5}$) for the whole set of measurement.

Monitoring these parameters during the self-discharge is used to bring some light into the origin of this phenomenon. The evolution of the fitted parameters with time and LMO Li content is presented in the S. inf. (Figs. 3 and 4 respectively). In addition, simple calculations [43] involving the Li content (x), the charge transfer resistance (R_{ct}), and the ionic resistance (R_{ion}) allow estimating the flow of incorporation of Li across the interface, $k \sim 1/xR_{ct}$, and the Li ion diffusivity in the LMO layer, $D \sim 1/xR_{ion}$ (see Fig. 5). According to this figure, the highest flow of Li incorporation ($k \sim 10^{-3}$ cm/s) is occurring at the beginning of the self-discharge process followed by a quick decay of almost two orders of magnitude in $\approx$12.5 h, then the incorporation flow is stabilized at $k \sim 3 \times 10^{-5}$ cm/s for the rest of the experiment, after $\approx$30 h.

As observed in Fig. 5, this short initial period is responsible for the insertion of ~75% of the total amount of Li incorporated in the
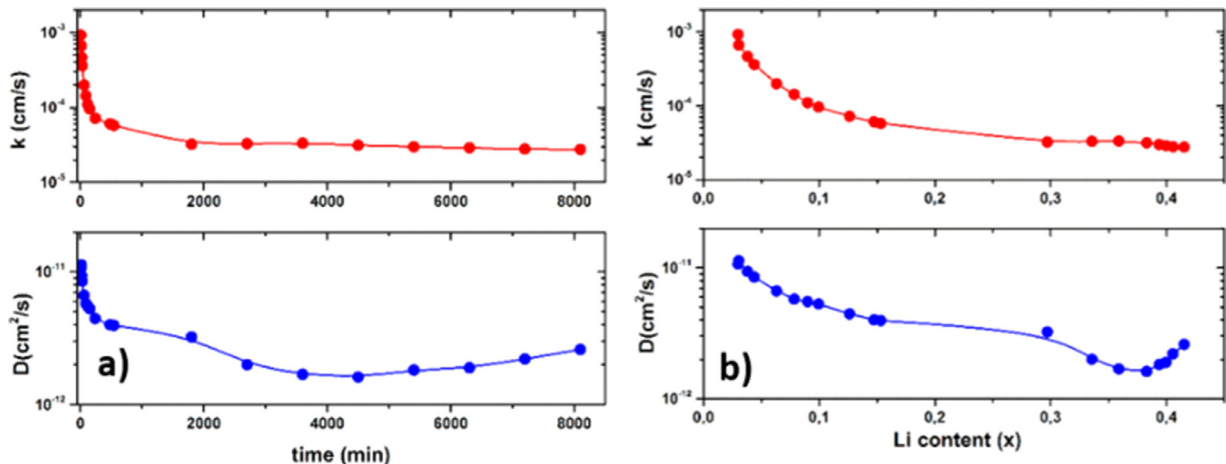

Fig. 5. Li-ion diffusivity (D) and exchange flow of lithium with the electrolyte (k) as a function of time (a) and the Li content (b) in the LMO.
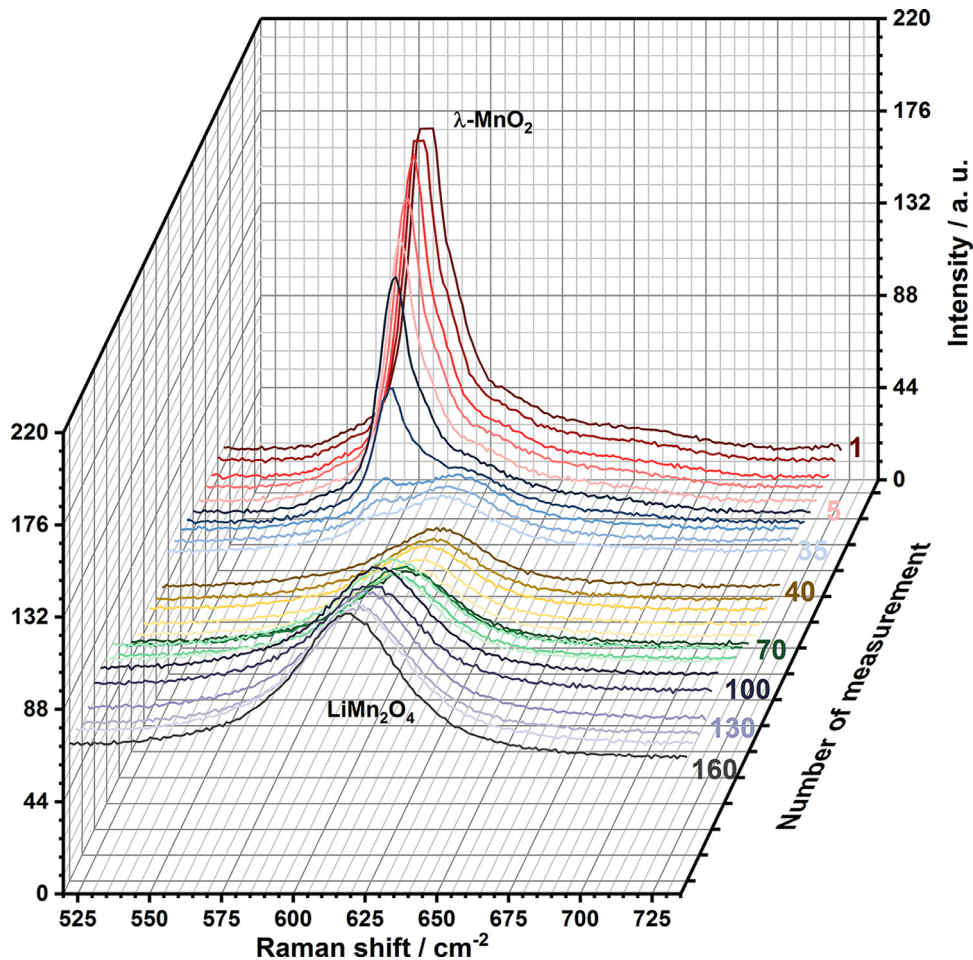
Fig. 6. Selected Raman spectra from the in-situ Raman analysis of LMO self-discharged OCV measurement. 1st, 2nd, 3rd, 4th, 5th, 6th, 15th, 25th, 30th, 35th, 40th, 45th, 50th, 60th, 65th, 70th, 75th, 80th, 100th, 110th, 130th, 140th, 150th, and 160th.

experiment, in agreement with Fig. 3, where 44% of the specific charge was lost after just 15 h and 75% after 30 h.

Together with the two-fold increase of the double layer capacitance in just one hour (Fig. 4a S. inf.), this strongly suggests after the formating of a Li-rich layer at the electrolyte-electrolyte interface, the self-discharge process is then drastically reduced. The initial parameters evolution revealed a similar trend to those obtained in classic studies when the composition is approaching to $Li_{0.5}Mn_2O_4$, half of the Li-ion 8a sites are occupied. On the other hand, several studies have proposed a lithiation mechanism based on Li-rich external and Li-poor bulk phases as well as the preferment lithiation and overlithiation of LMO particles surface than bulk were responsible for the degradation of the electrochemical behavior [52–55]. Similar to these publications, the trend observed in the parameters could be explained by the formation of a "Li-rich" surface (closed to $Li_{0.5}Mn_2O_4$). The absence of an external driving force could make that initially just the surface of the film was reactive and the impedance spectra evolution was representative of the approaching to the $Li_{0.5}Mn_2O_4$. At larger times, the evolution of the parameters was similar to the observed in previous impedance studies of LMO thin film at different states of charge (SOC) and dynamic impedance spectroscopy analysis. [56,57] The Li could diffuse deeper in the particle and the impedance spectra evolution was similar to obtained from the initial charge state to medium charge state ($0.5 \geq x \geq 0.1$). This behavior would be in agreement with the initial fast potential decay and high capacity losses and the moderating degrada-

tion at higher times (Fig. 3). However, the accumulation of Lithium at the surface cannot be simply associated with a slow diffusion within LMO after incorporation, since the here measured diffusivity ($D\sim10^{-11}$ cm^2/s at t=0) involves diffusion times ($t_D\sim$d^2/4D) of less than one minute (t_D=35s at t=0) for crossing the whole thickness of the electrode. Indeed, it is presumably occurring an initial lithium accumulation close to the current collector interface after crossing the whole electrode. This is supported by the strong increase of the associated capacitance (C_{cc}) during the first stage of the self-discharge experiment (from 10^{-4} to 10^{-2} F/cm^2). As expected, it is observed a decrease in the diffusivity from the empty λ-MnO$_2$ ($x\sim0$ at t=0) to the partially filled LMO follow by a small rise at the end of the experiment (t=130 h, see Fig. 5) when the Li content approached to 0.5 associated to the starting of the second reaction process, $Li_{0.5}Mn_{1.5}^{+4}Mn_{0.5}^{+3}O_4 + Li^+ \leftrightarrow Li_1Mn_1^{+4}Mn_1^{+3}O_4$, in agreement with previous studies that showed an increment of Li ion diffusivity at this stage [58].

The differences observed between the beginning and medium-large times could be attributed to the decay of potential. The lowering of potential probably caused a decreased oxidation capacity of the material to oxidize the water electrolyte and consequently to incorporate Li in its structure also hindering a further reduction of more Mn^{+4} to Mn^{+3}, reaching a maximum value of 0.43.

The self-discharge of an LMO aqueous battery was also monitored using in-situ Raman spectroscopy. The thin-film electrodes were oxidized to a cut off potential of 1.05 V vs Ag/AgCl (3 M KCl), then a Raman spectra composed of 160 scans were ob-

tained sequentially, and simultaneously the potential evolution was recorded (Fig. 6 and Fig. 4. S. Inf.). The time per scan was 5 min, then each spectrum can be associated to a determined potential in Fig. 4. S. Inf., (e. g. spectrum 40th = 200 min and equivalent to 0.87 V vs Ag/AgCl)

The potential profile observed (Fig. 5. S. Inf.) was different from the obtained in the above-described self-discharge study (Fig. 2.S. Inf.). The increment of temperature sample owing to the green light source exacerbated the self-discharge process. At a considerably lower resting time, the full λ-MnO$_2$ was converter into LMO. The two plateaus appeared in these circumstances, as shown in Fig. 5.S. Inf. It is well known that the effect of laser radiation can cause both a photo-excitation and an increase of the temperature, which both produce an acceleration of the discharge process [59]. In the same way, It has been demonstrated that the self-discharge of Li-ion batteries based on organic solvent can be abnormally accelerated even by their exposition to a routine short-term thermal exposure [35]. Fig. 6 shows selected Raman spectra from the in situ Raman analysis of LMO self-discharged OCV measurement. The complete number of spectrum recorded is included in Figure 7. S. Inf. A nearly complete transformation into the LMO phase was obtained after just 14 hours of OCV which clearly demonstrated the accelerating effect of the use of a green light source in the self-discharge of LMO. This laser could promote the degradation, forming compounds like Mn$_2$O$_3$ and Mn$_3$O$_4$ by chemical reactions photo-induced or thermal-induced. However, its influence in the SOC of Li-ion batteries is in general not considered that could have affected the results obtained owing to the acceleration of the SOD.

Despite this acceleration of self-discharge phenomena due to photonic or thermal excitation, the Raman spectra taken along the whole charge-state range provide information about the phase evolution of the layer, which has previously been studied by in-situ Raman and X-ray diffraction experiments. [60–62] A clear peak at c.a. 590 cm^{-1} is present in the nearly fully discharge states, which has been associated with the A$_{1g}$ mode of λ-MnO$_2$. [60] The high asymmetry produced by a shoulder at higher energy (c.a. 600 nm) has been attributed to the second peak of this same phase [63]. The remarkably higher intensity in this potential range is due to a resonance enhancement of the Raman spectrum for the delithiated spinel centered at c.a. 620 nm, which is not present in LMO [60,61]. At further discharge a broad peak centered at c.a. 610 cm^{-1} appears, which has been ascribed to two A1 and T2 modes of Li$_{0.5}$Mn$_2$O$_4$. Further Li$^+$ insertion towards LMO does not produce evident changes due to the similar peak positions, characterized by a peak at 628 cm^{-1} (A1g) with a shoulder around 595 cm^{-1}. The 628 cm^{-1} phonon is assigned to A1g of LMO [64]. A slight shift to higher frequencies and an increase of the peak intensity is however still observable at increased lithiation states, which is compatible with the progressive appearance of the LMO phase. Interestingly, the Raman peaks associated with λ-MnO$_2$ disappears after few cycles with a clear correlation with (i) first fast potential and charge losses, and (ii) evolution of the resistances and capacitances of the equivalent circuit in the first stages of discharge (Figs. 3 and 4). Whilst it is not possible to correlate the Li content with the amount of λ-MnO$_2$, it is plausible that the first fast discharge period comes from a higher exchange flow of lithium (Fig. 5) in agreement with the first region of potential decay observed in Fig. 3a.

4. Conclusions

In this study, the self-discharge process of the LMO spinel as a cathode electrode in Li-ion aqueous batteries was investigated. LMO thin films were prepared by a novel multi-targets Pulsed Laser Deposition approach. The films showed excellent electrochemical performances and fast kinetics. The self-discharge process was deeply studied through sequential Open Circuit Voltages measurements, increasing the resting times up to 135 h. The evolution of capacity losses and potential decay were monitored. A three regions behavior was observed with an initial very fast degradation (22.5 mVh^{-1} and 4.6% of total capacity per hour) followed by two zones with lower capacity and voltage fading (1.7 mVh^{-1} and 0.7 mVh^{-1}). The impedance study revealed two different evolutions of the electric parameters. At medium-high times, the classic evolution of the values of the resistors and capacitors related to the conversion from λ-MnO$_2$ to Li$_x$Mn$_2$O$_4$ was obtained, but at short times the changes were equivalent to the observed at electrode composition close to Li$_{0.5}$Mn$_2$O$_4$ instead of initial λ-MnO$_2$. This behavior was ascribed to the formation of a "Li-rich" surface of the film/particles owing to the absence of an external signal to impose the SOC similar to observed in overlithiathed and degraded Li-ion batteries. Finally, an in-situ Raman analysis of the self-discharge process confirmed the fast conversion of the oxidized form to the partially reduced phase and demonstrate the anomalous and faster self-discharge owing to the heating effect of the laser, equivalent to storage at high temperature, which accelerates the process.

The Li-ion aqueous batteries based on novel LMO materials with nanometric particles dimension and high surface are considered a "Second-Level Charge materials" with ultrafast and ultrahigh electrochemical performances. Their unique properties could also contribute to a fast self-discharge of the batteries, however, there are no studies that analyze this drawback. In this article we have demonstrated the easier self-discharge of LMO in aqueous media than in organic-based electrolytes, furthermore, we think that this degradation effect should be considered in future Li-ion aqueous cathode studies. This study opened new questions about the nature, composition, and mechanism of the self-discharge in aqueous media that will require deep and complex structural analysis like in-situ XPS or in-situ TEM which will permit analyze in detail the surface of the electrodes at initial times of self-discharge.

Declaration of Competing Interest

The authors declare that they have no known competing financial interests or personal relationships that could have appeared to influence the work reported in this paper.

Supplementary materials

Supplementary material associated with this article can be found, in the online version, at doi:10.1016/j.electacta.2021.137847.

References

[1] C.D. Wessells, R.A. Huggins, Y. Cui, Copper hexacyanoferrate battery electrodes with long cycle life and high power, Nat. Commun. 2 (2011).

[2] R. Trócoli, F. La Mantia, An aqueous zinc-ion battery based on copper hexacyanoferrate, ChemSusChem 8 (2015) 481–485.

[3] M.A. González, R. Trócoli, I. Pavlovic, C. Barriga, F. La Mantia, Layered double hydroxides as a suitable substrate to improve the efficiency of Zn anode in neutral pH Zn-ion batteries, Electrochem. Commun. 68 (2016) 1–4.

[4] G. Kasiri, R. Trócoli, A. Bani Hashemi, F. La Mantia, An electrochemical investigation of the aging of copper hexacyanoferrate during the operation in zinc-ion batteries, Electrochim. Acta 222 (2016) 74–83.

[5] R. Trócoli, G. Kasiri, F. La Mantia, Phase transformation of copper hexacyanoferrate (KCuFe(CN)6) during zinc insertion: effect of co-ion intercalation, J. Power Sources 400 (2018) 167–171.

[6] N. Alias, A.A. Mohamad, Advances of aqueous rechargeable lithium-ion battery: a review, J. Power Sources 274 (2015) 237–251.

[7] M. Jayalakshmi, M.M. Rao, F. Scholz, Electrochemical behavior of solid lithium manganate (LiMn$_2$O$_4$) in aqueous neutral electrolyte solutions, Langmuir 19 (2003) 8403–8408.

[8] A. Eftekhari, Electrochemical behavior of thin-film LiMn$_2$O$_4$ electrode in aqueous media, Electrochim. Acta 47 (2001) 495–499.

[9] M.M. Rao, et al., Electrochemical behaviour of solid lithium cobaltate (LiCoO$_2$) and lithium manganate (LiMn$_2$O$_4$) in an aqueous electrolyte system, J. Solid State Electrochem. 5 (2001) 50–56.

[10] J.W. Lee, S.Il Pyun, Investigation of lithium transport through LiMn2O4film electrode in aqueous LiNO3solution, Electrochim. Acta 49 (2004) 753–761.

[11] J.C. Arrebola, Á. Caballero, L. Hernán, J. Morales, Aqueous rechargeable lithium battery based on LiNi$_{0.5}$Mn$_{1.5}$O$_4$ spinel with promising performance, Energy Fuels 27 (2013) 7854–7857.

[12] W. Tang, et al., LiMn$_2$O$_4$ nanorods as a super-fast cathode material for aqueous rechargeable lithium batteries, Electrochem. Commun. 13 (2011) 1159–1162.

[13] W. Tang, et al., LiMn$_2$O$_4$ nanotube as cathode material of second-level charge capability for aqueous rechargeable lithium batteries, Nano Lett. 13 (2013) 2036–2040.

[14] W. Tang, et al., Nanochain LiMn$_2$O$_4$ as ultra-fast cathode material for aqueous rechargeable lithium batteries, Electrochem. Commun. 13 (2011) 205–208.

[15] W. Tang, et al., Nano LiMn$_2$O$_4$ as cathode material of high rate capability for lithium ion batteries, J. Power Sources 198 (2012) 308–311.

[16] W. Tang, et al., An aqueous rechargeable lithium battery of excellent rate capability based on a nanocomposite of MoO$_3$ coated with PPy and LiMn$_2$O$_4$, Energy Environ. Sci. 5 (2012) 6909–6913.

[17] Q. Qu, et al., Porous LiMn$_2$O$_4$ as cathode material with high power and excellent cycling for aqueous rechargeable lithium batteries, Energy Environ. Sci. 4 (2011) 3985–3990.

[18] Y.G. Wang, Y.Y. Xia, A new concept hybrid electrochemical surpercapacitor: carbon/LiMn$_2$O$_4$ aqueous system, Electrochem. 7 (2005) 1138–1142.

[19] O. Hanna, S. Luski, T. Brousse, D. Aurbach, Aqueous energy-storage cells based on activated carbon and LiMn$_2$O$_4$ electrodes, J. Power Sources 354 (2017) 148–156.

[20] L.J. Xi, et al., Single-crystalline Li$_4$Ti$_5$O$_{12}$ nanorods and their application in high rate capability Li$_4$Ti$_5$O$_{12}$/LiMn$_2$O$_4$ full cells, J. Power Sources 242 (2013) 222–229.

[21] F.X. Wang, et al., Spinel LiMn$_2$O$_4$ nanohybrid as high capacitance positive electrode material for supercapacitors, J. Power Sources 246 (2014) 19–23.

[22] S. Borhani-Haghighi, et al., Synthesis of nanostructured LiMn$_2$O$_4$ thin films by glancing angle deposition for Li-ion battery applications, Nanotechnology 27 (2016) 455402–455411.

[23] M. Fehse, et al., Ultrafast dischargeable LiMn$_2$O$_4$ thin-film electrodes with pseudocapacitive properties for microbatteries, ACS Appl. Mater. Interfaces 9 (2017) 5295–5301.

[24] R. Trócoli, et al., High specific power dual-metal-ion rechargeable microbatteries based on LiMn$_2$O$_4$ and zinc for miniaturized applications, ACS Appl. Mater. Interfaces 9 (2017) 32713–32719.

[25] R. Trócoli, A. Dushina, S. Borhani-Haghighi, A. Ludwig, F.La Mantia, Effect of Pt and Au current collector in LiMn$_2$O$_4$ thin film for micro- batteries effect of Pt and Au current collector in LiMn$_2$O$_4$ thin film for micro-batteries, Nanotechnology 29 (2018) 035440–035411.

[26] M. Fehse, et al., An innovative multi-layer pulsed laser deposition approach for LiMn$_2$O$_4$ thin film cathodes, Thin Solid Films 648 (2018) 108–112.

[27] G.M. Ehrlich, Linden's Handbook of Batteries, Fourth Edition, Handbook of Batteries, 2002.

[28] R. Yazami, Y. Ozawa, Probing the self-discharge current in LiMn$_2$O$_4$, LiCoO$_2$ and Li(NiMnCo) 1/3 O$_2$ cathodes, ECS Trans. 1 (2006) 151–159.

[29] R. Yazami, Y. Ozawa, A kinetics study of self-discharge of spinel electrodes in Li/Li xMn$_2$O$_4$ cells, J. Power Sources 153 (2006) 251–257.

[30] N. Nakayama, et al., Interfacial lithium-ion transfer at the LiMn$_2$O$_4$ thin film electrode/aqueous solution interface, J. Power Sources 174 (2007) 695–700.

[31] A. Blyr, et al., Cells in their discharged state understanding by means of three--electrode measurements, J. Electrochem. Soc. 145 (1998) 194–209.

[32] S. Zhang, M.S. Ding, T.R. Jow, Self-discharge of Li/LixMn$_2$O$_4$ batteries in relation to corrosion of aluminum cathode substrates, J. Power Sources 102 (2001) 16–20.

[33] R. Wang, X. Li, Z. Wang, H. Guo, Manganese dissolution from LiMn$_2$O$_4$ cathodes at elevated temperature: methylene methanedisulfonate as electrolyte additive, J. Solid State Electrochem. (2016), doi:10.1007/s10008-015-2998-1.

[34] A. Blyr, A.Du Pasquier, G. Amatucci, J.-M Tarascon, Origin of self-discharge mechanism in LiMn$_2$O$_4$-based Li-ion cells: a chemical and electrochemical approach, Ionics (Kiel) 3 (1997) 321–331.

[35] W.M. Seong, et al., Abnormal self-discharge in lithium-ion batteries, Energy Environ. Sci. 11 (2018) 970–978.

[36] X. Tang, et al., Investigation of the self-discharge behaviors of the LiMn$_2$O$_4$ cathode at elevated temperatures: in situ X-ray diffraction analysis and a co-doping mitigation strategy, J. Mater. Chem. A 7 (2019) 13364–13371.

[37] A. Konarov, Self-discharge of Rechargeable Hybrid Aqueous Battery, Waterloo, 2014.

[38] G. Zampardi, R. Trocoli, W. Schuhmann, F. La Mantia, Revealing the electronic character of the positive electrode/electrolyte interface in lithium-ion batteries, Phys. Chem. Chem. Phys. 19 (2017) 28381–28387.

[39] J. Stojadinovic, A. Dushina, R. Trõcoli, F. La Mantia, Electrochemical characterization of gel electrolytes for aqueous lithium-ion batteries, Chempluschem 79 (2014) 1507–1511.

[40] D.M. Robinson, Y.B. Go, M. Greenblatt, G.C. Dismukes, Water oxidation by λ-MnO$_2$: catalysis by the cubical Mn$_4$O$_4$ subcluster obtained by delithiation of spinel LiMn$_2$O$_4$, J. Am. Chem. Soc. 132 (2010) 11467–11469.

[41] C.W. Cady, et al., Tuning the electrocatalytic water oxidation properties of AB$_2$O$_4$ spinel nanocrystals: a (Li, Mg, Zn) and B (Mn, Co) site variants of LiMn$_2$O$_4$, ACS Catal. 5 (2015) 3403–3410.

[42] F.M. Balci, et al., Synthesis of mesoporous LiMn$_2$O$_4$ and LiMn$_2$-xCoxO$_4$ thin films using the MASA approach as efficient water oxidation electrocatalysts, J. Mater. Chem. A 6 (2018) 13925–13933.

[43] J. Jamnik, J. Maier, Generalised equivalent circuits for mass and charge transport: chemical capacitance and its implications, Phys. Chem. Chem. Phys. 3 (2001) 1668–1678.

[44] J. Bisquert, G. Garcia-Belmonte, F. Fabregat-Santiago, P.R. Bueno, Theoretical models for ac impedance of finite diffusion layers exhibiting low frequency dispersion, J. Electroanal. Chem. 475 (1999) 152–163.

[45] R. Trócoli, J. Morales, S. Franger, J. Santos-Peña, Influence of the lithium salt electrolyte on the electrochemical performance of copper/LiFePO$_4$ composites, Electrochim. Acta 61 (2012) 57–63.

[46] R. Trócoli, S. Franger, J. Morales, J. Santos-Peña, Insights on the electrode/electrolyte interfaces in LiFePO$_4$ based cells with LiAl(Al) and Li(Mg) anodes, J. Electroanal. Chem. 732 (2014) 53–60.

[47] R. Trócoli, M. Cruz-Yusta, J. Morales, J. Santos-Peña, On the limited electroactivity of Li$_2$NiTiO$_4$ nanoparticles in lithium batteries, Electrochim. Acta 100 (2013) 93–100.

[48] M.G.S.R. Thomas;, P.G.B.J.B Goodenough, AC impedance analysis of polycrystalline insertion electrodes: application to Li1 − x CoO$_2$, J. Electrochem. Soc. 132 (1985) 1521–1528.

[49] S. Franger, S. Bach, J. Farcy, J.P. Pereira-Ramos, N. Baffier, An electrochemical impedance spectroscopy study of new lithiated manganese oxides for 3 V application in rechargeable Li-batteries, Electrochim. Acta 48 (2003) 891–900.

[50] C.A.C. Sequeira, A. Hooper, The study of lithium electrode reversibility against (PEO)xLiF3CSO3 polymeric electrolytes, Solid State Ion. 10 (1983) 1131–1138.

[51] D. Fauteux, Institut de recherched'Hydro-2u-bec, 1800, MonrOe SteJulie, Varennes, Quebec, Canada, JOL 2PO, Solid State Ion. 17 (1985) 133–138.

[52] Kosilov, V. V, Potapenko, A. V & Kirillov, S. A. Effect of overdischarge (overlithiation) on electrochemical properties of LiMn2O4 samples of different origin. (2017) doi:10.1007/s10008-017-3671-7.

[53] W. Liu, K. Kowal, G. C. F. Mechanism of the Electrochemical Insertion of Lithium into LiMn$_2$O$_4$ Spinels, J. Electrochem. Soc. 145 (1998) 459–465.

[54] D. Tang, et al., Surface structure evolution of LiMn$_2$O$_4$ cathode material upon charge/discharge, Chem. Mater. 26 (2014) 3535–3543 2014.

[55] M.M. Thackeray, C.S. Johnson, J.T. Vaughey, N. Li, S.A. Hackney, Advances in manganese-oxide ' composite ' electrodes for lithium-ion batteries, J. Mater. Chem. 15 (2005) 2257–2267.

[56] M. Mohamedi, et al., Explicit analysis of impedance spectra related to thin films of spinel LiMn$_2$O$_4$, J. Power Sources 93 (2001) 93–103.

[57] C. Erinmwingbovo, V. Siller, M. Nuñez, R. Trócoli, D. Brogioli, A. Morata, F. La Mantia, Dynamic impedance spectroscopy of LiMn$_2$O$_4$ thin films made by multilayer pulsed laser deposition, Electrochim. Acta 331 (2020) 135385.

[58] J. Xie, et al., Li-ion diffusion kinetics in LiMn$_2$O$_4$ thin films prepared by pulsed laser deposition, Electrochim. Acta 54 (2008) 376–381.

[59] H. Search, C. Journals, A. Contact, M. Iopscience, Raman spectroscopic studies of lithium manganates with spinel structure, J. Phys. Condens. Matter 15 (2003) 3151–3162.

[60] B. Ammundsen, G.R. Burns, M.S. Islam, H. Kanoh, J. Rozière, Lattice dynamics and vibrational spectra of lithium manganese oxides: a computer simulation and spectroscopic study, J. Phys. Chem. B 103 (1999) 5175–5180.

[61] K. Dokko, Q. Shi, I.C. Stefan, D.A Scherson, In situ raman spectroscopy of single microparticle Li +-intercalation electrodes, J. Phys. Chem. B 107 (2003) 12549–12554.

[62] T. Eriksson, A.-K. Hjelm, G. Lindbergh, T. Gustafsson, Kinetic study of {LiMn}[sub 2]O[sub 4] cathodes by in situ {XRD} with constant-current cycling and potential stepping, J. Electrochem. Soc. 149 (2002) A1164.

[63] Q. Shi, Y. Takahashi, J. Akimoto, I.C. Stefan, D.a. Scherson, In Situ raman scattering measurements of a LiMn$_2$O$_4$ single crystal microelectrode, Electrochem. Solid-State Lett. 8 (2005) A521.

[64] C.M. Julien, M. Massot, Lattice vibrations of materials for lithium rechargeable batteries III. Lithium manganese oxides, Mater. Sci. Eng. B Solid-State Mater. Adv. Technol. 100 (2003) 69–78.